

Chiral symmetry restoration in the three-dimensional four-fermion model at non-zero temperature and density

J.B. Kogut and C.G. Strouthos

Department of Physics, University of Illinois at Urbana-Champaign, Urbana, Illinois 61801-3080

The three-dimensional four-fermion model with a Z_2 chiral symmetry and $N = 4$ fermion species in the system is investigated numerically at non-zero temperature T and chemical potential μ . The phase diagram in the (T, μ) plane is mapped out quantitatively. A detailed finite size scaling analysis shows that the $T = 0, \mu \neq 0$ chiral phase transition is first order, whereas the $T \neq 0, \mu \neq 0$ transition remains second order down to very low T . Quantitative results for the location of the end of the first order line are given.

I. INTRODUCTION

The chiral phase transition in QCD separating high temperature (high density) quark-gluon plasma phase from low temperature (low density) hadronic phase has been studied intensively in the last decade. At temperatures of the order of the pion mass, $T \approx 140$ MeV or densities a few times that of ordinary nuclear matter, $n \approx (3-5)n_0$ with $n_0 \approx 0.15 \text{ fm}^{-3}$, conditions are reached where hadrons start overlapping, only the short distance interaction among the internal parton degrees of freedom described by QCD is important and dynamical breaking of chiral symmetry no longer occurs. Understanding the properties of this transition is becoming increasingly important in view of recent experimental efforts to create and detect the quark-gluon plasma in the relativistic heavy-ion collisions at BNL and CERN.

Since the problem of chiral symmetry breaking and its restoration is intrinsically non-perturbative, the number of available techniques is limited and most of our knowledge about the phenomenon comes from lattice simulations. Due to the complexity of QCD, studies have so far been done on lattices of modest size and have been unable to yield quantitative results as far as the universality class of the finite temperature phase transition is concerned. Also, finite density QCD, which is more relevant to real physics, is a field where lattice technology is still at an early stage [1]. The complex nature of the determinant of the Dirac operator at finite chemical potential makes it impossible to use standard simulation algorithms based on positive definite probability functions.

This manuscript addresses the problem of chiral symmetry restoration at non-zero temperature and non-zero chemical potential in the three-dimensional four-fermion model * [2,3] with a Z_2 chiral symmetry in order to understand what ingredients might play a decisive role in more complex systems like gauge theories. The model has been simplified as much as possible in order to produce data of the highest quality and get some insight into the range of parameters we need for studies of more realistic problems. The large N description (which is equivalent to a mean field approximation) of the phase structure of the three-dimensional

*In this work we shall use the terms “four-fermion model” and “Gross-Neveu model” interchangeably when it concerns a theory with a four-fermion interaction in $2+1$ dimensions.

four-fermion model at non-zero chemical potential [4] predicts a first order transition for $T = 0$ and a continuous transition for $T > 0$. The critical value of the chemical potential μ_c is equal to the value of the fermion mass at $\mu = 0$. Interactions as expected decrease μ_c below the mean field result [5]. A recent numerical study [6] of the $T \neq 0, \mu = 0$ transition favors the two-dimensional Ising model exponents for $N < \infty$. In this manuscript we present the results of Monte Carlo simulations with a small number of fermion species, i.e., $N = 4$ in order to test the mean field theory predictions and look for possible next-to-the-leading order corrections. We show in this paper by employing finite size scaling techniques that the $T = 0, \mu \neq 0$ phase transition is first order. We also show that the second order nature of the $T \neq 0, \mu = 0$ transition remains stable down to low temperatures and high values of the chemical potential. A simple continuity argument suggests that a tricritical point in the (T, μ) plane must lie on the low temperature and high density section of the critical line. More specifically, our simulations show that the tricritical point lies on the section of the phase boundary defined by: $T/T_c \leq 0.23$, $\mu/\mu_c \geq 0.97$, where T_c is the zero density critical temperature and μ_c is the zero temperature critical chemical potential. Our results show that higher order corrections in the $1/N$ expansion for the location of the transition points in the phase diagram are very small for this model.

II. THE MODEL

The continuum spacetime (we work in Euclidean space throughout) Lagrangian of the model is

$$\mathcal{L} = \bar{\psi}_i (\not{\partial} + \mu \gamma_0 + m_q) \psi_i - \frac{g^2}{2N} (\bar{\psi}_i \psi_i)^2. \quad (1)$$

Here ψ_i is a four-component spinor and the index i runs over N fermion species, μ is the chemical potential and m_q is the fermion bare mass. For zero fermion bare mass, \mathcal{L} has a Z_2 chiral symmetry

$$\psi \rightarrow \gamma_5 \psi ; \bar{\psi} \rightarrow -\bar{\psi} \gamma_5 \quad (2)$$

which is spontaneously broken whenever a non-vanishing condensate $\langle \bar{\psi} \psi \rangle$ is generated. Both analytical and numerical work in this model are aided by the introduction of an auxiliary field σ , so Eq. (1) becomes

$$\mathcal{L} = \bar{\psi}_i (\not{D} + \sigma + m_q) \psi_i + \frac{N}{2g^2} \sigma^2. \quad (3)$$

At tree level, the field σ has no dynamics; it is truly an auxiliary field. However, it acquires dynamical content by dint of quantum effects arising from integrating out the fermions. In the chiral limit the vacuum expectation value of σ becomes a dynamical fermion mass and it is a convenient order parameter for any chiral phase transition in the theory.

There are several motivations for studying such a simple model: (i) for sufficiently strong coupling it exhibits chiral symmetry breaking at zero temperature and density; (ii) the spectrum of excitations contains both baryons and mesons, ie. the elementary fermions and the composite fermion–anti-fermion states; (iii) the model has an interacting continuum limit; (iv) when formulated on the lattice it has a real Euclidean action even for non-zero chemical potential; (v) the Yukawa-like coupling makes the inverse Dirac operator non-singular and the simulations can be done in the chiral limit directly, whereas in gauge theories the matrix to be inverted becomes ill-conditioned and the simulations have to be done using a fermion bare mass; (vi) the model has fewer degrees of freedom than QCD, and can be studied with greater precision on much bigger lattices than the lattices presently used for QCD thermodynamics. The chiral symmetry must be discrete in order to observe a phase transition at non-zero temperature in $d = 2 + 1$, otherwise according to Coleman-Mermin-Wagner theorem [7] a continuous chiral symmetry must be manifested algebraically for all $T > 0$.

In four dimensions the four-fermion model is a trivial theory and is believed to be an effective theory of quarks and gluons at intermediate energies. Unfortunately, the order of the chiral phase transition at non-zero chemical potential in this model depends on the value of the cutoff [8]. In two dimensions the discrete chiral symmetry restoration is dominated by the materialization of kink–anti-kink states. The zero temperature and finite chemical potential transition is first order, whereas for any finite number of fermion species N the chiral symmetry is restored at any non-zero temperature due to the condensation of the kinks [9].

The Gross-Neveu model in its bosonized form may be formulated on a spacetime lattice using the following action:

$$S_{lat} = \sum_{i=1}^{N/2} \left(\sum_{x,y} \bar{\chi}_i(x) M_{x,y} \chi_i(y) + \frac{1}{8} \sum_x \bar{\chi}_i(x) \chi_i(y) \sum_{\langle \tilde{x}, x \rangle} \sigma(\tilde{x}) \right) + \frac{N}{4g^2} \sum_{\tilde{x}} \sigma^2(\tilde{x}), \quad (4)$$

where χ_i and $\bar{\chi}_i$ are Grassmann-valued staggered fermion fields defined on the lattice sites, the auxiliary field σ is defined on the dual lattice sites [10], and the symbol $\langle \tilde{x}, x \rangle$ denotes the set of 8 dual lattice sites \tilde{x} surrounding the direct lattice site x . The lattice spacing a has been set to one for convenience. Details and motivation of this particular scheme can be found in [3]. The fermion kinetic operator M is given by

$$M_{x,y} = \frac{1}{2} \left[e^\mu \delta_{y,x+\hat{0}} - e^{-\mu} \delta_{y,x-\hat{0}} \right] + \frac{1}{2} \sum_{\nu=1,2} \eta_\nu(x) [\delta_{y,x+\hat{\nu}} - \delta_{y,x-\hat{\nu}}], \quad (5)$$

where $\eta_\nu(x)$ are the Kawamoto-Smit phases $(-1)^{x_0+\dots+x_{\nu-1}}$. The influence of the chemical potential μ is manifested through the timelinks following [11]. Only fermion loops which wrap around the timelike direction are affected by its inclusion. The energy density ϵ , and the fermion number density n , are defined by

$$\epsilon = -\frac{1}{V_s} \frac{\partial \ln Z}{\partial T^{-1}} = \frac{1}{V} \text{tr} \partial_o \gamma_o S_F = \frac{1}{2V} \langle \sum_x e^\mu M_{x,x+\hat{0}}^{-1} - e^{-\mu} M_{x,x-\hat{0}}^{-1} \rangle, \quad (6)$$

$$n = -\frac{T}{V_s} \frac{\partial \ln Z}{\partial \mu} = \frac{1}{V} \text{tr} \gamma_o S_F = \frac{1}{2V} \langle \sum_x e^\mu M_{x,x+\hat{0}}^{-1} + e^{-\mu} M_{x,x-\hat{0}}^{-1} \rangle. \quad (7)$$

Here Z is the partition function of the model, V_s is the spatial volume and $V = V_s/T$ the overall volume of spacetime. The final expression in each case is the quantity measured in the simulation, using a noisy estimator to calculate the matrix inverses.

The cubic lattice has L_s lattice spacings a in spatial directions and L_t lattice spacings in the temporal direction. The momentum cutoff scale can be defined as $\Lambda = 1/a$, the temperature is given by $T = 1/(L_t a)$ and the mass of the sigma meson is $m = 1/(\xi a)$, where ξ is the correlation length of the sigma field. To reach a continuum limit one has to satisfy the following two conditions: $\Lambda \gg T$ and $\Lambda \gg m$. The condition $\Lambda \gg T$ requires a lattice with sufficiently large $L_t \gg 1$. The parameters of the action should then be tuned towards their critical values where the correlation length $\xi \gg 1$. This satisfies the condition $\Lambda \gg m$.

III. MONTE CARLO SIMULATIONS

We performed Monte Carlo simulations of the Gross-Neveu model in $d = 2 + 1$ dimensions to study its phase structure in the (T, μ) plane. We used a hybrid Monte Carlo method

described in [3], which proved to be very efficient for our purposes. Since the chiral symmetry is discrete we were able to simulate the model directly in the chiral limit, i.e., setting the fermion bare mass to zero. The three-dimensional character of the model and its relatively simple form allowed us to perform simulations on large lattices and generate a large number of trajectories relative to state-of-the-art lattice QCD simulations. This allowed a particularly accurate determination of the order of the phase transition at various points in the (T, μ) plane. In order to check whether it is possible to detect next-to-the-leading order corrections to the large N calculation we set $N = 4$. This is the smallest number of fermion species allowed by the hybrid Monte Carlo algorithm, because in order to have a positive semi-definite fermionic determinant, N must be a multiple of four.

We used the following two methods to optimize the performance of the hybrid Monte Carlo procedure. The first method consisted of tuning the effective number of fermion flavors N' , which is used during the integration of the equations of motion along a microcanonical trajectory, so as to maximize the acceptance rate of the Monte Carlo procedure for a fixed microcanonical time-step $d\tau$. As the lattice size was increased, the time step $d\tau$ had to be taken smaller and the optimal N' approached N . For example, for the $N = 4$ theory on a 16×32^2 lattice the choices $d\tau = 0.12$ and $N' = 4.026$ gave acceptance rates greater than 90% for all couplings of interest. To maintain this acceptance rate on a 16×64^2 lattice we used $d\tau = 0.10$ and $N' = 4.018$. In the second method the Monte Carlo procedure was optimized by choosing the trajectory length τ at random from a Poisson distribution with the mean equal to $\bar{\tau}$. This method of optimization, which guarantees ergodicity, was found to decrease autocorrelation times dramatically [12]. For most of our runs we used the average trajectory length $\bar{\tau} \simeq 2.0$. As usual, the errors were calculated by the jackknife blocking, which accounts for correlations in a raw data set.

A. $\mu = 0, T = 0$

In this section we present the results of the simulations at zero temperature and zero chemical potential. The purpose of these simulations is to determine the scaling window of the $T = 0, \mu = 0$ theory. The knowledge of the scaling window is necessary in order to ensure that the value of the lattice coupling $\beta \equiv 1/g^2$ used in the simulations at non-zero

temperature and density is sufficiently close to the bulk critical coupling β_c , which means that lattice artifacts are negligible. In other words, we verified that another important physical parameter, the zero-temperature mass, m_0 , is sufficiently smaller than the cutoff Λ . We ran on large symmetric lattices, such as 20^3 with $N = 4$ for $\beta = [0.500, 0.750]$ and determined the magnetic critical exponent β_{mag} by fitting the values of the order parameter $\Sigma_0 \equiv \langle \sigma \rangle$ to the scaling relation $\Sigma_0 = A(\beta_c - \beta)^{\beta_{mag}}$. We found that $\beta_c \approx 0.845$ and $\beta_{mag} = 1.00(2)$ which is in agreement with the analytical prediction $\beta_{mag} = 1 + \mathcal{O}(1/N^2)$ for the $T = 0, \mu = 0$ scaling [3]. According to the graph in Fig. 1, the range of β for which the (Σ_0, β) points fall on the ‘scaling’ line is $\beta \approx [0.55, 0.75]$. This confirms that for these values of the coupling the lattice theory remains in the scaling window for all range of temperatures down to $T = 0$ and effects of the lattice are negligible.

B. $\mu \neq 0, T = 0$

In this section we discuss the results from numerical simulations of the three-dimensional four-fermion model with $N = 4$ at non-zero chemical potential and zero temperature. The mean field theory approximation [4] predicts that the finite μ phase transition is everywhere second order except at the isolated point $T = 0$. The issue raised by our lattice simulations in this section is whether the first order nature of the transition predicted by mean field theory at $T = 0$ persists, when the theory has a small number of fermion species. In addition these simulations are motivated by our interest to study the difficulties in determining the order of the transition using detailed finite size scaling methods. We simulated the system at $\beta = 0.625$ because this value of β is deep in the broken phase and is also in the scaling window of the bulk critical point which means we can extract continuum physics from these simulations by standard methods. The order parameter for these simulations is defined by: $\Sigma \equiv \langle |\sigma| \rangle$. The absolute value of σ is necessary in order to take into account tunneling between the degenerate Z_2 -symmetric vacua when the parameters are tuned close to the transition. In the thermodynamic limit $\Sigma \rightarrow \langle \sigma \rangle$.

Figure 2 shows the order parameter Σ versus μ for fixed $\beta = 0.625$ on $16^3, 22^3, 30^3$ and 40^3 lattices. The values of Σ on the bigger lattices show no μ dependence until μ reaches the vicinity of the critical chemical potential μ_c . The variation of Σ becomes more abrupt

as the volume of the system increases, indicating that a step-function type singularity will develop in the infinite volume. The data on the 40^3 lattice show a jump discontinuity in Σ as μ varies from 0.3850 to 0.3875. The fermion number density n and the energy density E are plotted in Figs. 3 and 4 as a function of μ for various lattice sizes. The transition at $\mu_c \approx 0.3850$ is seen equally well in these quantities. Furthermore, the variations of n and E near the transition become more abrupt as the volume increases, indicating again that a step-function singularity will develop in the thermodynamic limit. It is clear from the behavior of the various observables that relatively large lattices are required to simulate the theory's actual critical behavior. The discontinuous transition seen on a 40^3 lattice is replaced by a relatively smooth curve on the 16^3 lattice.

Our simulations were unable to distinguish a possible nuclear matter liquid-gas transition from the chiral transition. The data in Fig. 3 for n versus μ show only one phase transition at μ_c . The smooth tail in the density before the transition is a finite size effect which dies out as the volume of the system increases. The nuclear matter liquid-gas transition coincides with the chiral transition in the large N approximation [4]. This implies that for $N = 4$ the next-to-the-leading order corrections are very small if not zero, in the sense that either the two transitions are very close or the nuclear matter liquid-gas transition is so weak that is smoothed out by finite volume effects. New simulations on volumes much larger than 40^3 are required in order to detect the nuclear matter liquid-gas transition.

Another interesting indicator to determine the order of the transition was proposed by Binder *et al.* [13], namely the reduced cumulant of the bosonic action S defined by

$$B_S = 1 - \frac{\langle S^4 \rangle}{3\langle S^2 \rangle^2}. \quad (8)$$

This quantity should approach $\frac{2}{3}$, if the distribution of the energy is described by a single Gaussian form with the width vanishing at infinite volume, such as in the case of a second order transition; otherwise it deviates from this value. In practice we calculate the quantity B_S for several values of the chemical potential near the transition for each of several lattice sizes. Then a plot of B_S versus chemical potential is made for each lattice size. An accurate value of $B_{S,min}$ for each lattice size is determined and then $B_{S,min}$ is plotted versus $\frac{1}{V}$. If the transition is second order, this plot should have a y-intercept (representing the infinite volume limit) approaching the value of two-thirds. In order to locate $B_{S,min}$ accurately we

performed simulations at very small intervals of μ near the transition. We accumulated approximately 30,000 to 40,000 trajectories for the various lattice sizes at each value of μ near μ_c . The cumulant as a function of μ is plotted in Fig. 5 for $L = 16, 18, 22, 30$. In Fig. 6 we plot $B_{S,min}$ versus inverse volume $\frac{1}{V}$. The straight line in Fig. 6 represents the best linear fit to the data and its y-intercept is equal to $0.66475(14)$, which is distinctly different from the value of $\frac{2}{3}$, indicating clearly that the model has a first order finite density and zero temperature phase transition. A similar result was obtained from the analysis of the reduced cumulant behavior of the energy density.

C. $\mu \neq 0, T \neq 0$

In this section we present the results from the simulations of the Gross-Neveu model at non-zero temperature and chemical potential. The purpose of these simulations is to study the phase structure of the model in the (T, μ) plane. The large N result predicts a second order phase transition for $T > 0$. We varied T by changing either the lattice temporal extend L_t or the lattice spacing a which vanishes when the coupling β is tuned to its ($T = \mu = 0$) critical value $\beta_c \approx 0.845$.

In Fig. 7 we plot the normalized values of the order parameter Σ/Σ_0 as a function of μ/Σ_0 at different values of T . The normalization of Σ and μ with the $T = \mu = 0$ value of the order parameter Σ_0 at the same value of the coupling β is essential in order to convert these quantities into physical units by getting rid of the lattice spacing. This enables us to compare the behavior of the order parameter as a function of the chemical potential at different temperatures on lattices with different lattice spacings. The parameters for the curves in Fig. 7 from left to right in terms of $(\beta, \text{ lattice shape})$ are: $(0.70, 8 \times 48^2)$, $(0.65, 8 \times 48^2)$, $(0.65, 16 \times 48^2)$, $(0.55, 16 \times 48^2)$, $(0.625, 40^3)$. It is clear from the shapes of these curves that the transition becomes sharper as we decrease the temperature and increase the chemical potential. In Fig. 8 we map out the phase diagram of the model in the $(T/\Sigma_0, \mu/\Sigma_0)$ plane.

After having determined the order of the phase transition at zero temperature (see previous section), we extended our work to determine the order of the transition at the two points of Fig. 8 with the lowest non-zero values of T . At these points which have parameters

$(L_t = 16, \beta = 0.65)$ and $(L_t = 16, \beta = 0.55)$, the variation of Σ/Σ_0 as a function of μ/Σ_0 is very sharp near the transition.

We first present the results for the order parameter Σ , the fermion number density n and the energy density E for the $L_t = 16, \beta = 0.65$ simulations in Figs. 9, 10, 11 respectively. These figures show a marked contrast with the corresponding ones at $T = 0, \mu \neq 0$ discussed in the previous section. In particular, in Fig. 9 an asymptotic curve is approached from above without mutual crossings of curves for different size, in contrast to Fig. 2. The variations of n and E in Figs. 10 and 11 also approach an asymptotic behavior without showing signs that a step-function-type singularity will develop in the thermodynamic limit. The non-zero fermion number density n before the transition does not depend on L_s . This means that the tail in n is not a finite L_s effect. It is instead a finite L_t or non-zero temperature effect. We have also estimated the reduced cumulants B_S for the bosonic action and B_E for the internal energy. For an accurate determination of these quantities we accumulated 30,000 to 50,000 trajectories for the various lattices near μ_c . We plot B_S and B_E versus μ in Figs. 12 and 13 respectively. Figure 14 shows the minimum values of the cumulants as functions of the inverse volume. The straight lines in Figs. 12 and 13 represent the best linear fits to the data and their y-intercepts are: 0.66667(3) for the action cumulant and 0.66668(3) for the energy cumulant. This analysis confirms our previous observation that the transition with $L_t = 16$ and $\beta = 0.65$ is a second order transition.

In order to study the phase structure of the model at lower temperatures we kept $L_t = 16$ and increased the lattice spacing by changing the coupling to $\beta = 0.55$. According to the discussion in Sec. III A the lattice discretization effects cannot be neglected for smaller values of β . We performed the new simulations on lattices with spatial extents $L_s = 32, 40, 48, 64$. The order parameter Σ , and the fermion number density n and the energy density E are plotted as functions of μ in Figs. 15, 16, 17. The variation of the thermodynamic observables is very sharp near the transition and it is therefore very difficult to distinguish between a weak first order and a second order transition. In order to learn more about the order of the transition we calculated again the reduced cumulants for the action and the energy density. For an accurate determination of these quantities we accumulated 90,000 to 120,000 trajectories for the various lattices near μ_c . B_S and B_E are plotted versus μ in Figs. 18 and

19. In Fig. 20 we plot the minima of the cumulants versus the inverse volume. The y-intercepts of the best linear fits give: 0.66628(13) for the action cumulant and 0.66641(13) for the energy cumulant. This analysis favors a very weak first order transition although the possibility of a second order transition cannot be excluded decisively. Studies on lattices with much larger temporal extends are required in order to probe very low temperatures and see a clear signal of a first order phase transition. Nevertheless, the steep variation of the thermodynamic quantities near the transition at $\beta = 0.55$ and $L_t = 16$, together with the small deviations of the thermodynamic limit of the cumulants' minima from the 2/3 value gives evidence that the system is close to its tricritical point.

IV. CONCLUSIONS

In this manuscript we presented the results of Monte Carlo simulations of the three-dimensional four-fermion model with $N = 4$ fermion species at non-zero temperature and density. With the exception of confinement this model incorporates most of the essential properties of QCD. The great advantage of this model is that it is possible to perform lattice simulations at non-zero chemical potential. We demonstrated using finite size scaling techniques that the $\mu \neq 0$, $T = 0$ phase transition is a first order transition. Our analysis did not succeed to distinguish the nuclear matter liquid-gas transition from the chiral phase transition. Either the two transitions are extremely close for the $N = 4$ theory or the nuclear matter liquid-gas transition which is expected before the chiral transition is very weak and is smoothed out by finite volume effects.

We have also shown that the second order nature of the $T \neq 0$, $\mu = 0$ phase transition remains stable for $T/T_c > 0.23$ and $\mu/\mu_c < 0.97$. This imples that the large N approximation (or mean field theory description of the transition) which predicts a second order phase transition everywhere except at the isolated point $T = 0$ [4] describes the order of the transition on the largest part of the critical line in the (T, μ) plane. In this sense the model has a “soft” behavior on the biggest section of the critical line. It should be noted that the mean field approximation does not predict the correct two-dimensional Ising universality class [6] of the second order phase transitions line. In that case non-perturbative effects are crucial in the critical region and the mean field results are modified by $1/N$ corrections.

However, the results of this study show that corrections to the large N limit for other characteristics of the model, including the position of the tricritical point and the position of the nuclear matter liquid-gas transition, are very small indeed.

A simple continuity argument implies that the model has a tricritical point on the critical line at a low temperature and very high density. Although our simulations at low T and high μ provided some evidence that the phase transition there might be a weak first order transition, studies on lattices with much larger temporal extent enabling us to probe sufficiently low temperatures would be required to “locate” the tricritical point unambiguously. Various approaches to QCD with two massless quarks at finite temperature and density suggest the existence of a tricritical point on the boundary of the phase with spontaneously broken chiral symmetry. The position of the tricritical point in two-flavor QCD was estimated recently using a random matrix model [14] and a Nambu–Jona-Lasinio model [15] as $T_{tr} \approx 100$ MeV and $\mu_{tr} \approx 600 - 700$ MeV. Possible experimental signatures suggested in [16] should allow future experiments at RHIC and LHC to provide information about the location and properties of the tricritical point.

Another conclusion drawn from our work is that lattices with very large spatial extends are needed in order to observe the order of the transition. Our studies on small volumes highlight the difficulties that must be faced when trying to understand the critical behavior of the thermodynamic limit by extrapolation from systems away from this limit. It was also shown that qualitative signatures of a first order phase transition such as the variation of various thermodynamic quantities near the transition can be very misleading unless they are accompanied by detailed finite size scaling analyses. This should be a warning to the lattice community that a quantitative understanding of the critical behavior of QCD at non-zero chemical potential lies along a difficult road.

ACKNOWLEDGEMENTS

Discussions with Misha Stephanov and Pavlos Vranas are greatly appreciated. This work was supported in part by NSF grant PHY96-05199. The computer simulations were done on the Cray C90’s and J90’s at NERSC and on the NOW at SDSC.

REFERENCES

- [1] I.M. Barbour *et al.*, Nucl. Phys. A (Proc. Suppl.) **60**, 220 (1998).
- [2] B. Rosenstein, B.J. Warr and S.H. Park, Phys. Rep. **205**, 59 (1991).
- [3] S. Hands, A. Kocic, J.B. Kogut Ann. Phys. **224**, 29 (1993).
- [4] S.J. Hands, A. Kocic and J.B. Kogut, Nucl. Phys. **B390**, 355 (1993).
- [5] S. Hands, S. Kim and J.B. Kogut, Nucl. Phys. **B442**, 364 (1995).
- [6] J.B. Kogut, M.A. Stephanov and C.G. Strouthos, Phys. Rev. **D58**, 096001 (1998).
- [7] S. Coleman, Comm. Math. Phys. **31**, 259 (1966); N.D. Mermin and H. Wagner, Phys. Rev. Lett. **17**, 1133 (1966).
- [8] S.P. Klevansky, Rev. Mod. Phys. **64**, 649 (1992).
- [9] U. Wolff, Phys. Lett. **B157**, 303 (1985); F. Karsch, J. Kogut and H.W. Wyld, Nucl. Phys. **B280**, 289 (1987).
- [10] Y. Cohen, S. Elitzur and E. Rabinovici, Nucl. Phys. **B220**, 102 (1983).
- [11] J.B. Kogut, H. Matsuoka, S.H. Shenker, J. Shigemitsu, D.K. Sinclair, M. Stone and H.W. Wyld, Nucl. Phys. **B225** [FS9], 93 (1983); P. Hasenfratz and F. Karsch, Phys. Lett. **B125**, 308 (1993).
- [12] S.J. Hands, A. Kocic, J.B. Kogut, R.L. Renken, D.K. Sinclair, and K.C. Wang, Nucl. Phys. **B413** (1994) 503.
- [13] K. Binder and D.P. Landau, Phys. Rev. **B30**, 1477 (1984).
- [14] M.A. Halasz, A.D. Jackson, R.E. Shrock, M.A. Stephanov and J.J.M. Verbaarschot, Phys. Rev. **D58**, 096007 (1998).
- [15] J. Berges and K. Rajagopal, Nucl. Phys. **B538**, 215 (1999).
- [16] M. Stephanov, K. Rajagopal and E. Shuryak, Phys. Rev. Lett. **81**, 4816 (1998); hep-ph/9903292

FIGURES

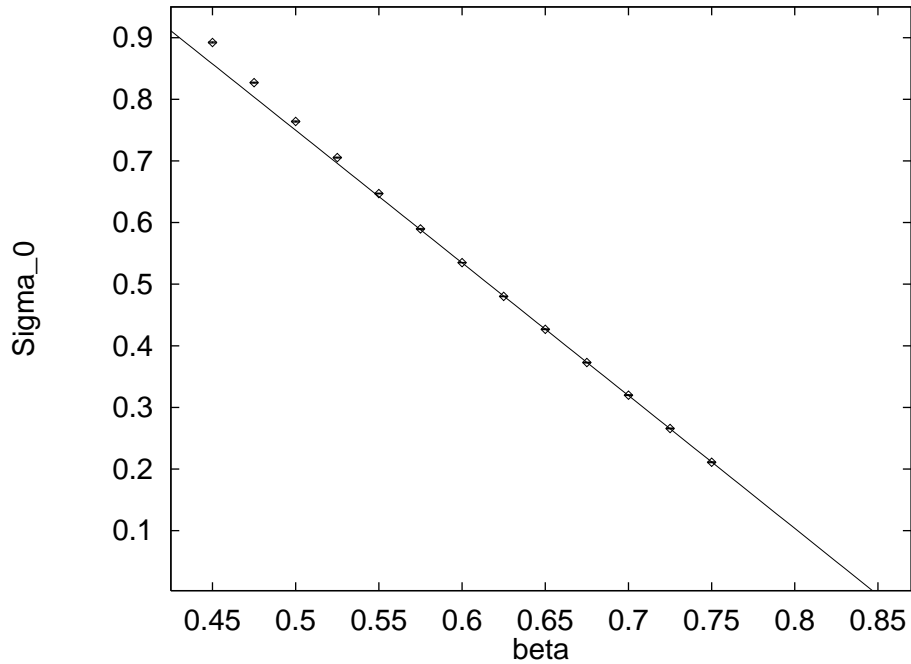


FIG. 1. Order parameter Σ_0 vs. β at $T = \mu = 0$.

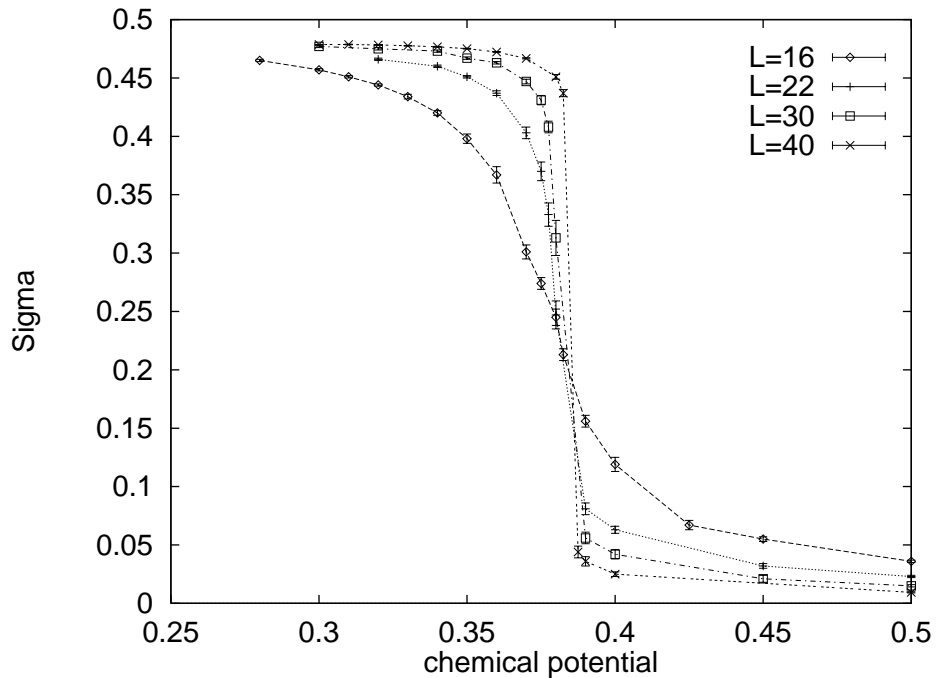


FIG. 2. Order parameter Σ vs. μ at $T = 0$ for $L = 16, 22, 30, 40$. The lines are not χ^2 fits; they connect the various points to guide the eye.

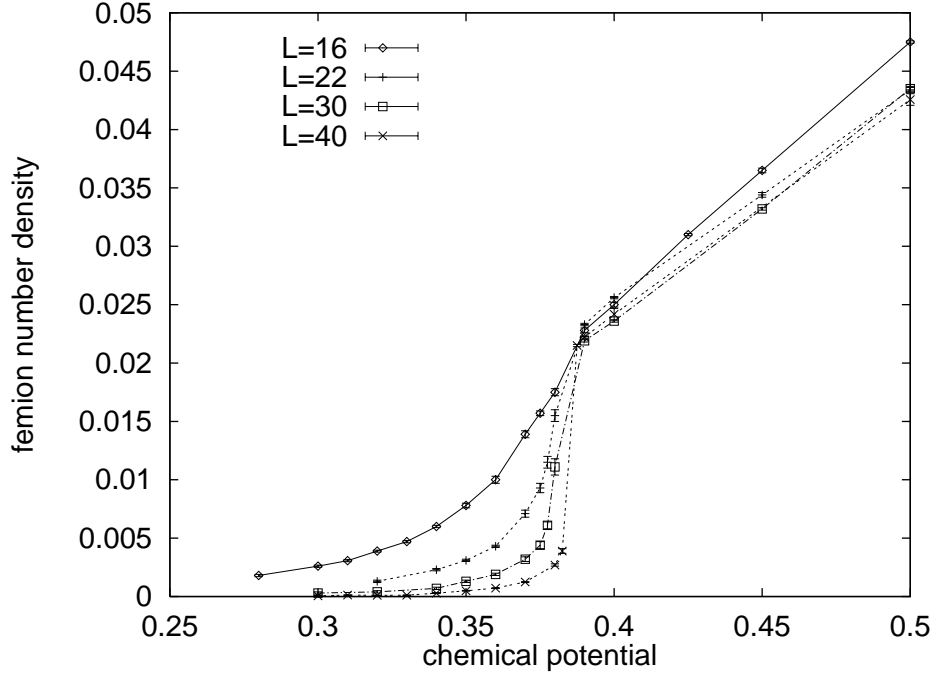


FIG. 3. Fermion number density n vs. μ at $T = 0$ for $L = 16, 22, 30, 40$. The lines are not χ^2 fits; they connect the various points to guide the eye.

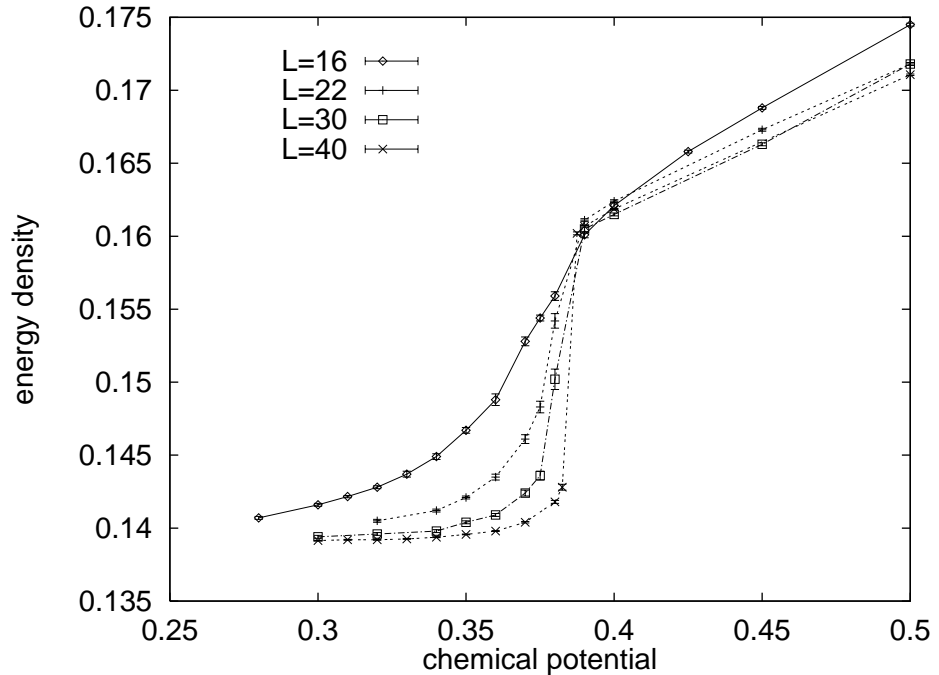


FIG. 4. Energy density E vs. μ at $T = 0$ for $L = 16, 22, 30, 40$. The lines are not χ^2 fits; they connect the various points to guide the eye.

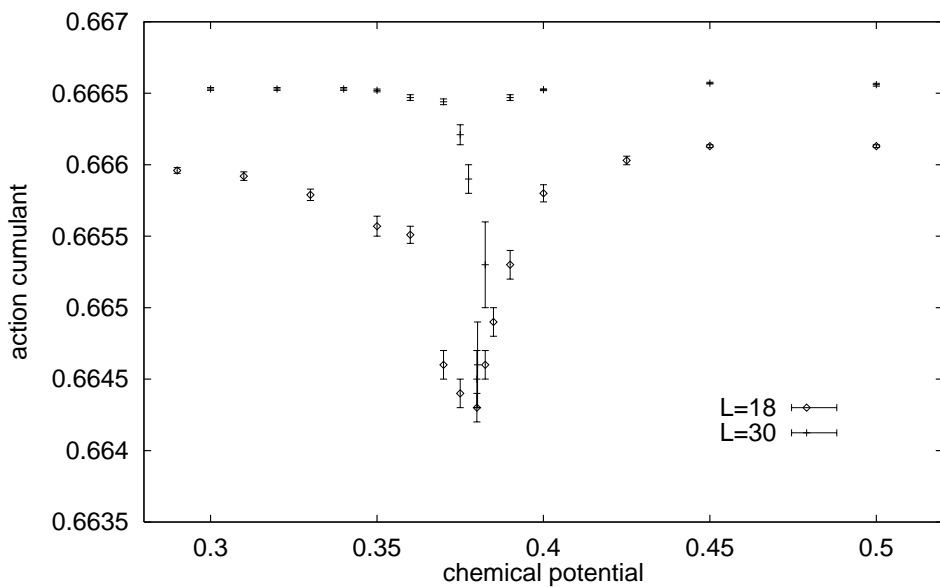
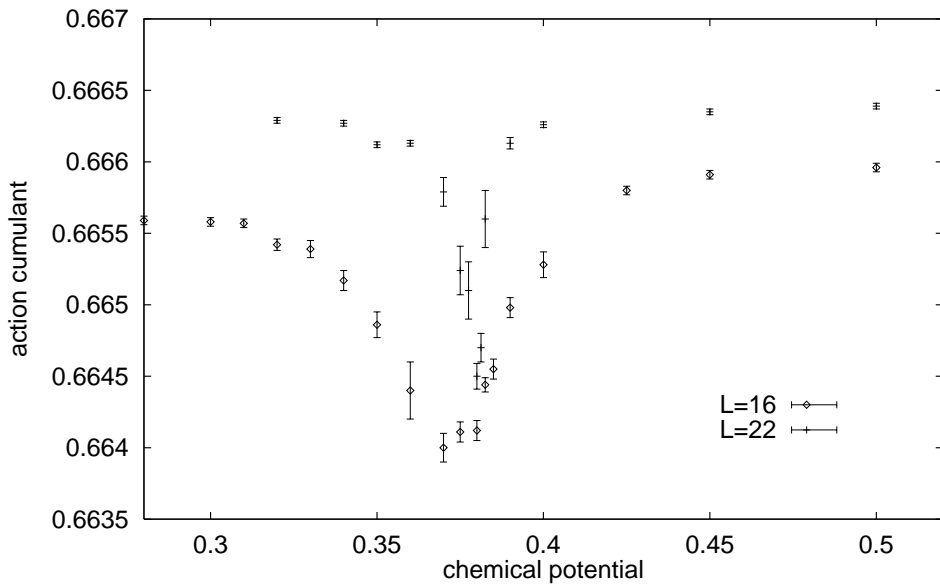


FIG. 5. The action cumulant B_S vs. μ at $T = 0$ for $L = 16, 18, 22, 30$.

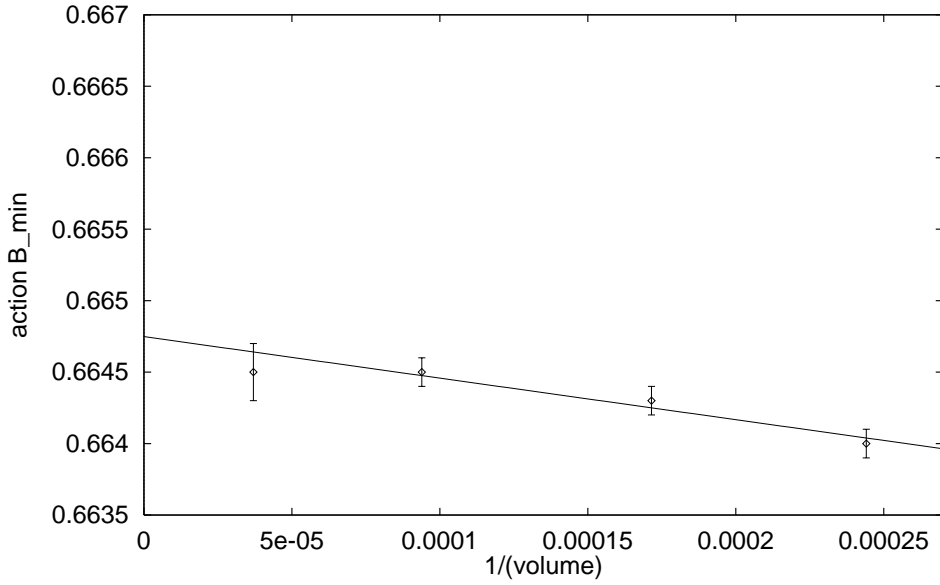


FIG. 6. The minimum values of the action cumulant B_S vs. inverse volume at $T = 0$. The solid line represents the best linear fit to the data.

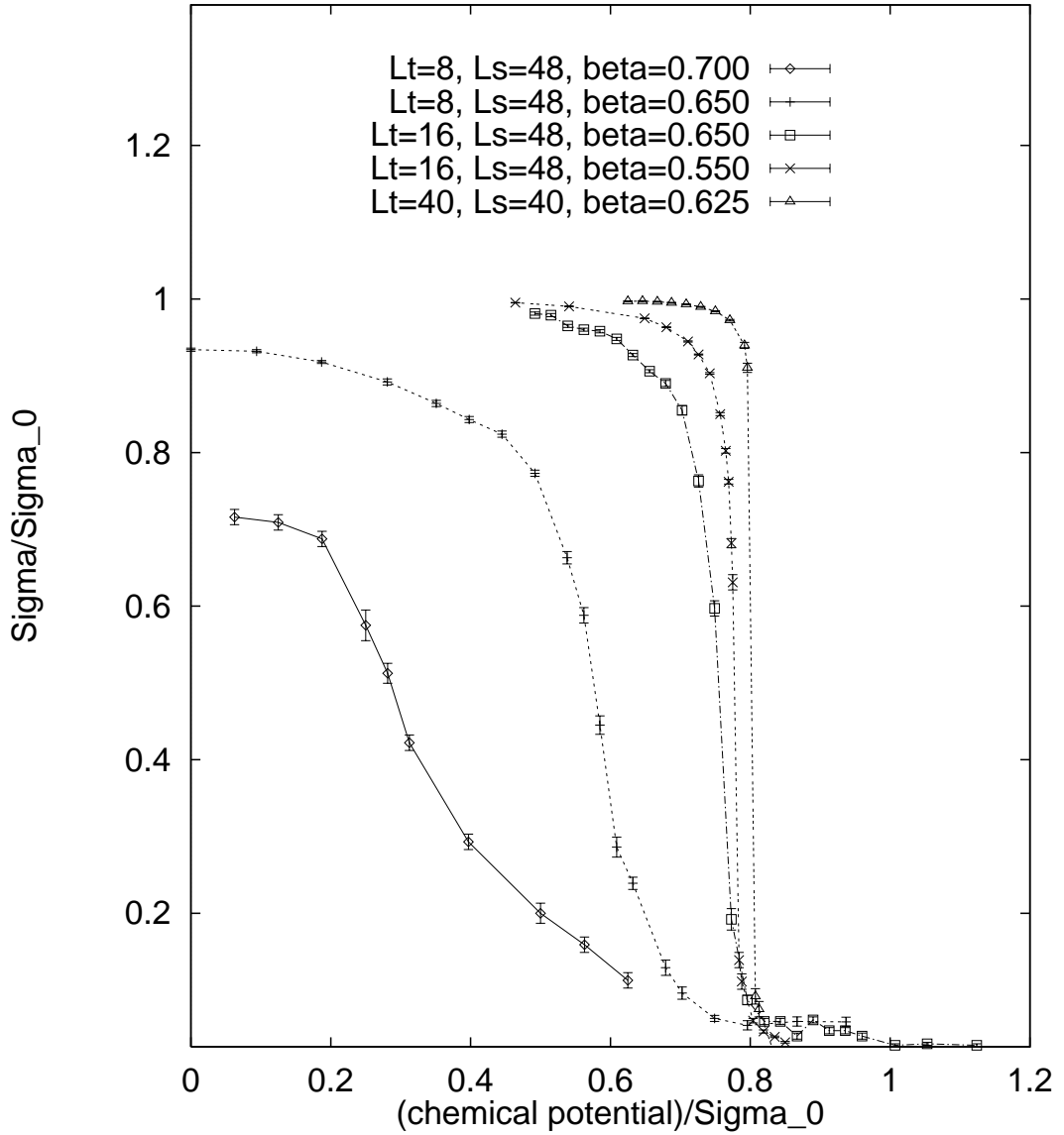


FIG. 7. Σ/Σ_0 vs. μ/Σ_0 for different values of temperature T . T decreases from left to right.

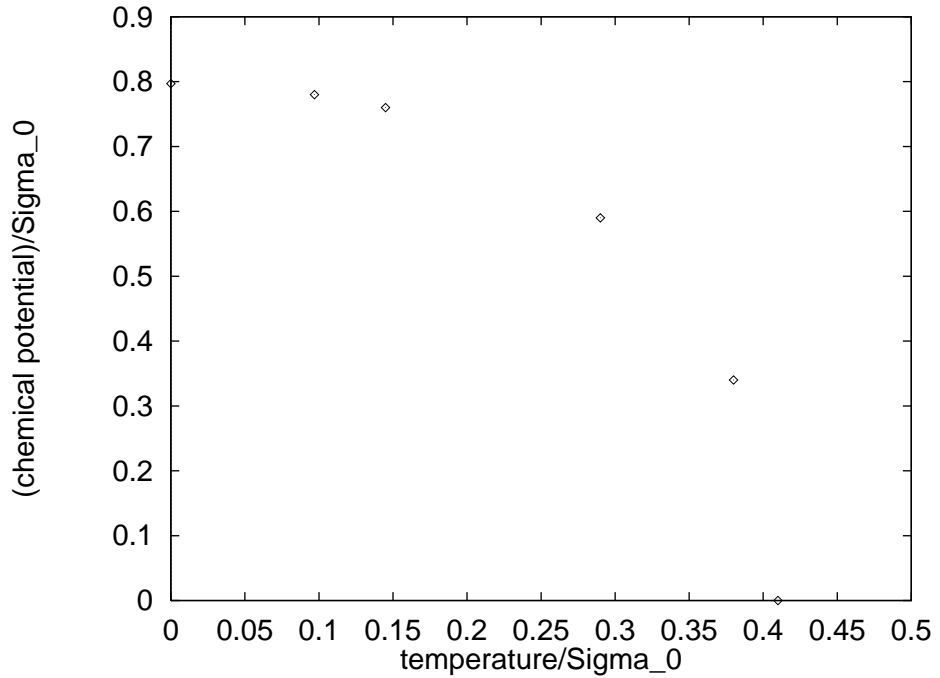


FIG. 8. Phase diagram of the $N = 4$ theory in the $(T/\Sigma_0, \mu/\Sigma_0)$ plane.

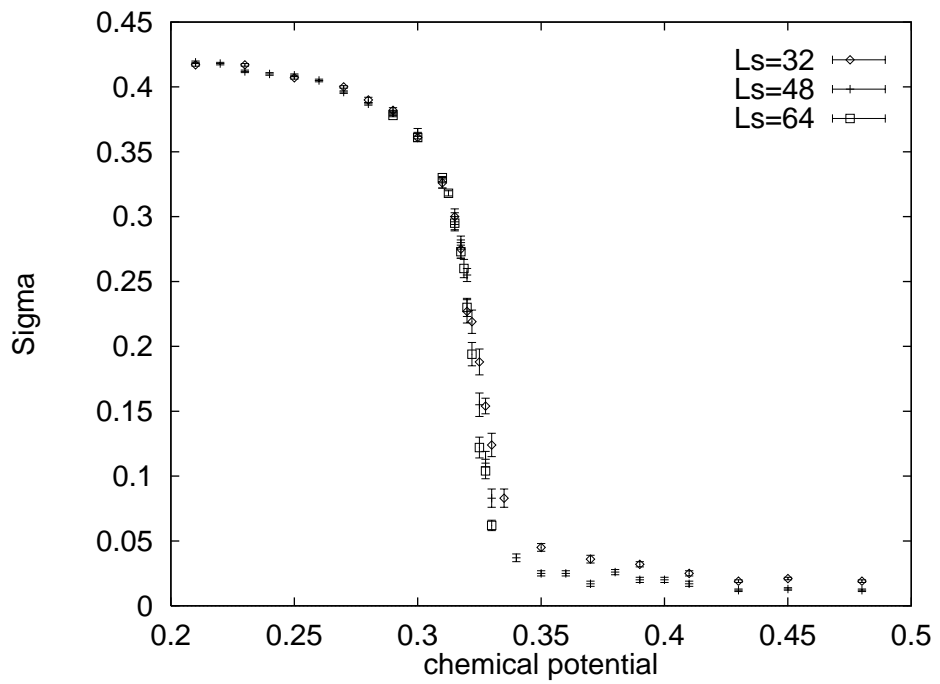


FIG. 9. Σ vs. μ for $L_t = 16$, $\beta = 0.65$ and $L_s = 32, 48, 64$.

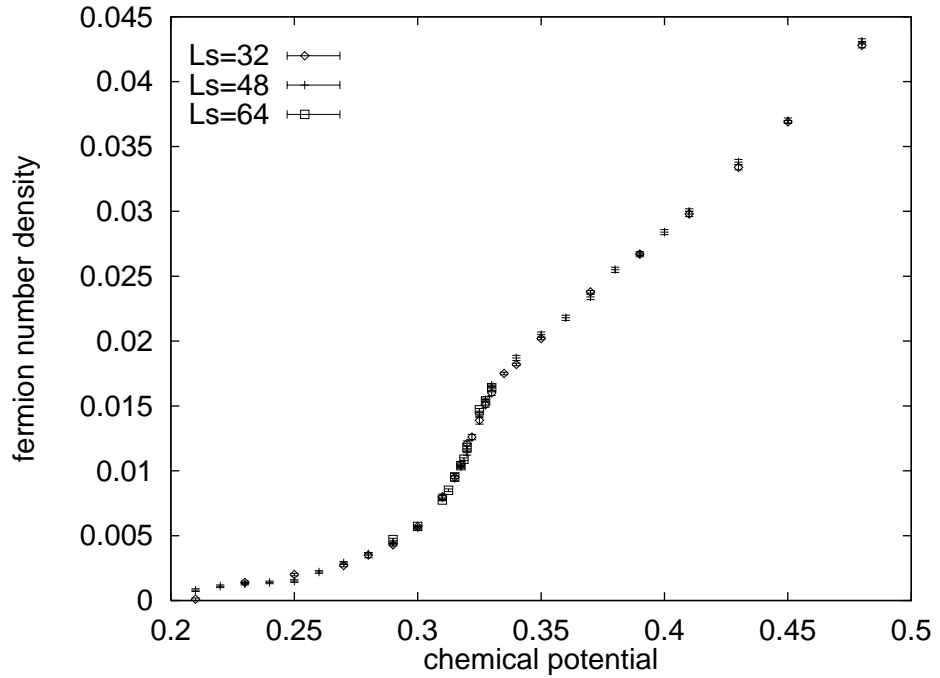


FIG. 10. Fermion number density n vs. μ for $L_t = 16$, $\beta = 0.65$ and $L_s = 32, 48, 64$.

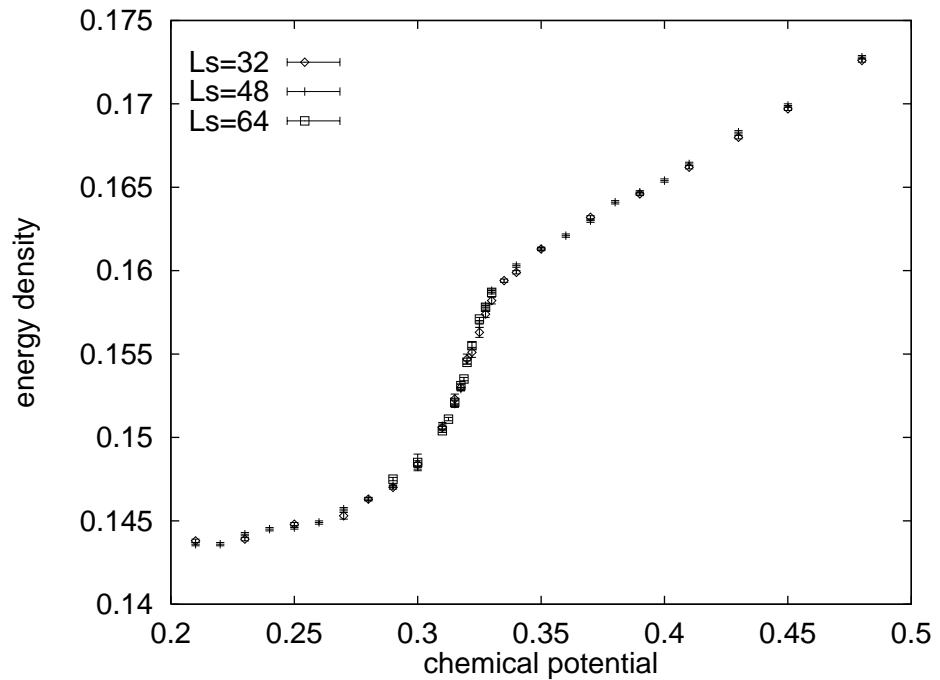


FIG. 11. Energy density E vs. μ for $L_t = 16$, $\beta = 0.65$ and $L_s = 32, 48, 64$.

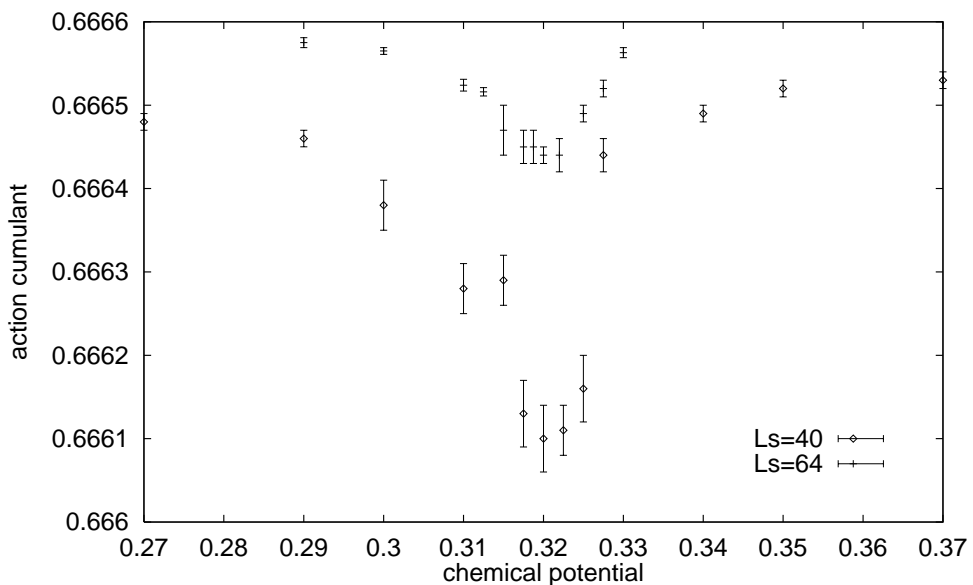
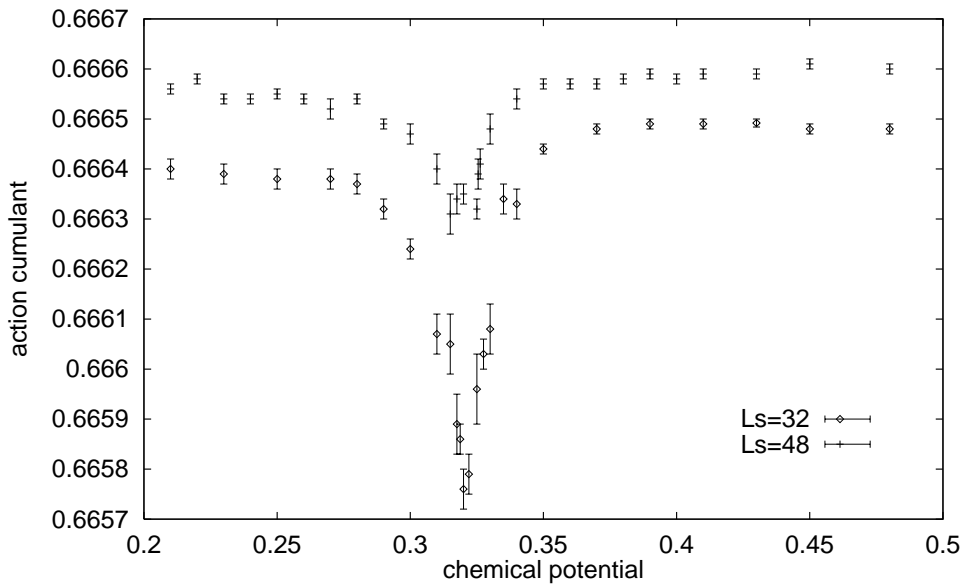


FIG. 12. The action cumulant B_S vs. μ for $L_t = 16$, $\beta = 0.65$ and $L_s = 32, 40, 48, 64$

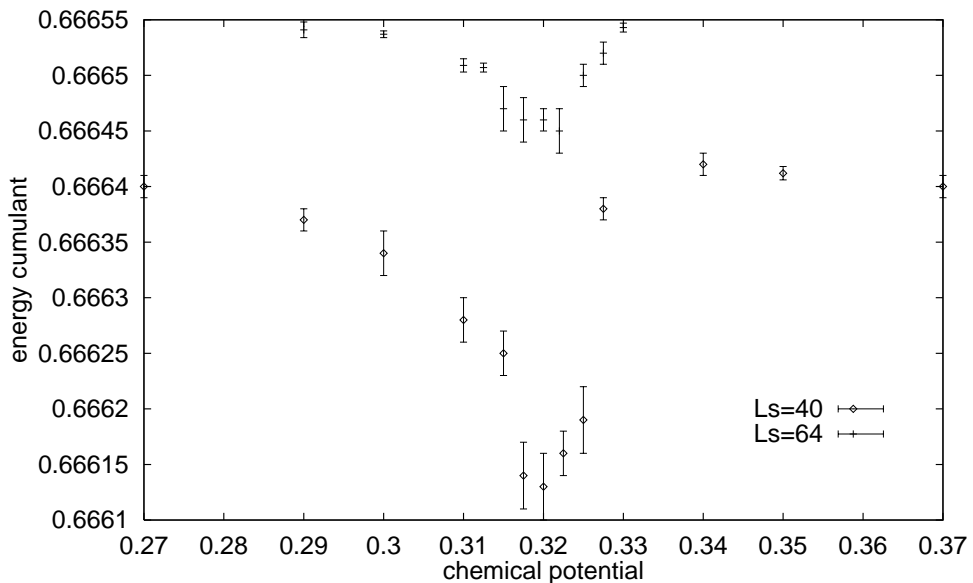
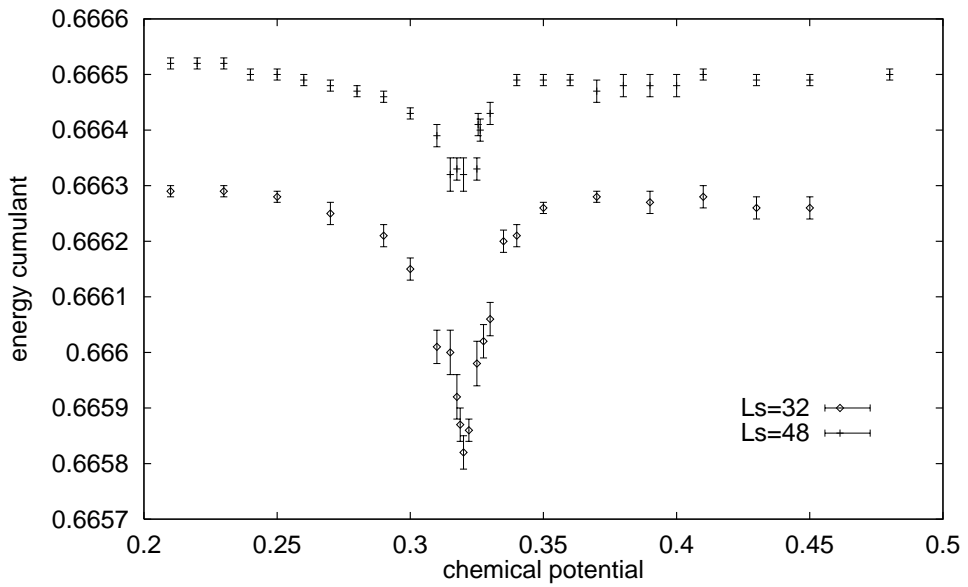


FIG. 13. The energy cumulant B_E vs. μ for $L_t = 16$, $\beta = 0.65$ $L_s = 32, 40, 48, 64$.

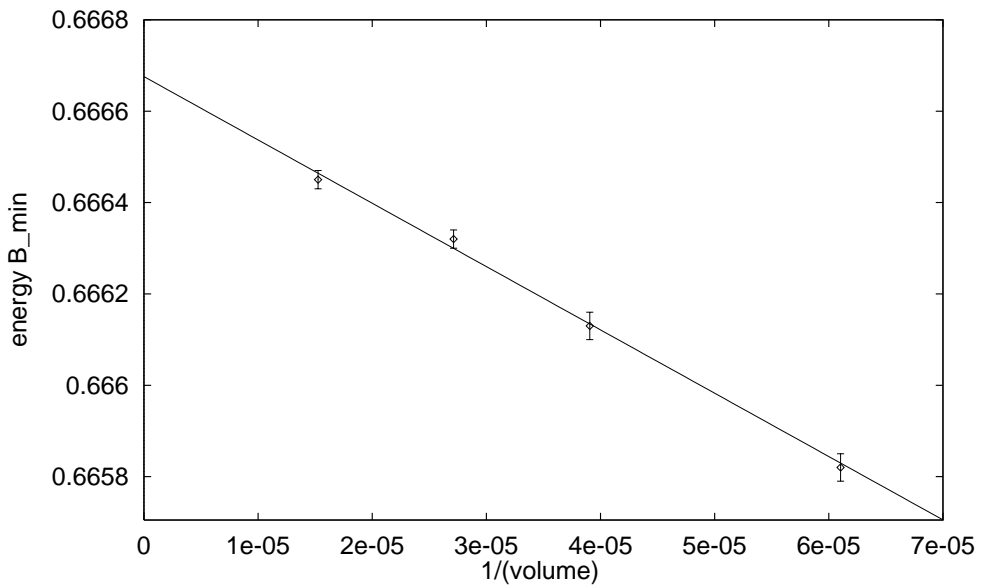
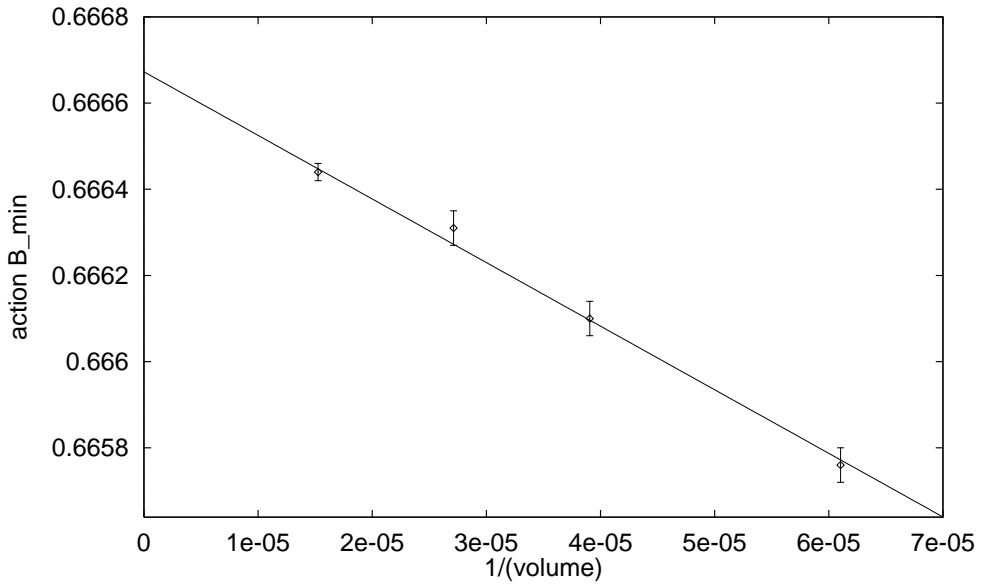


FIG. 14. The minimum values of the action and energy cumulants vs. inverse volume for $L_t = 16$, $\beta = 0.65$. The solid lines represent the best linear fits to the data.

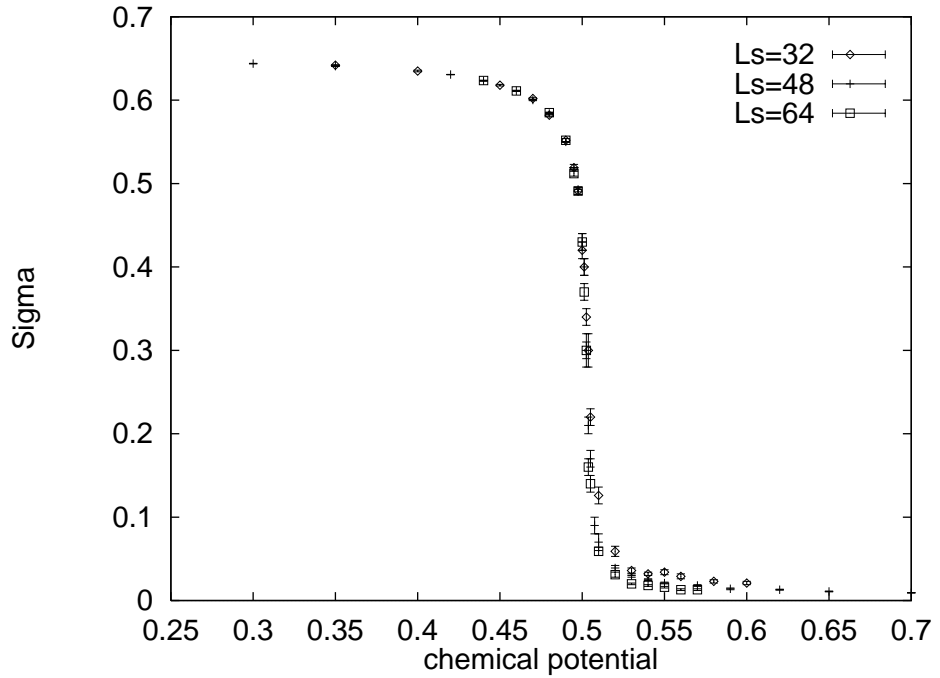


FIG. 15. Σ vs. μ for $L_t = 16$, $\beta = 0.55$ and $L_s = 32, 48, 64$.

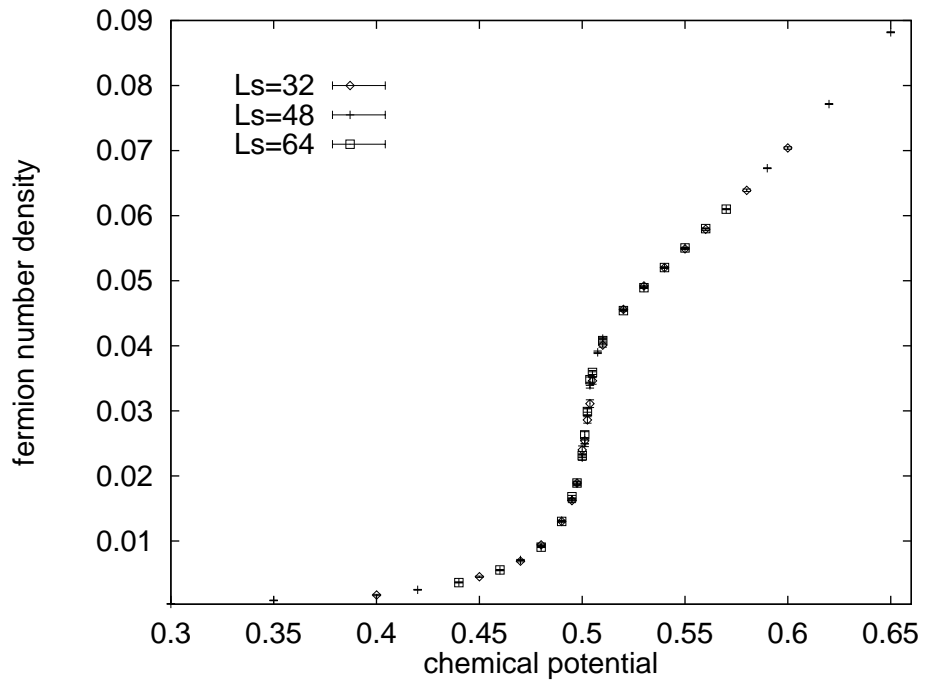


FIG. 16. Fermion number density n vs. μ for $L_t = 16$, $\beta = 0.55$ and $L_s = 32, 48, 64$.

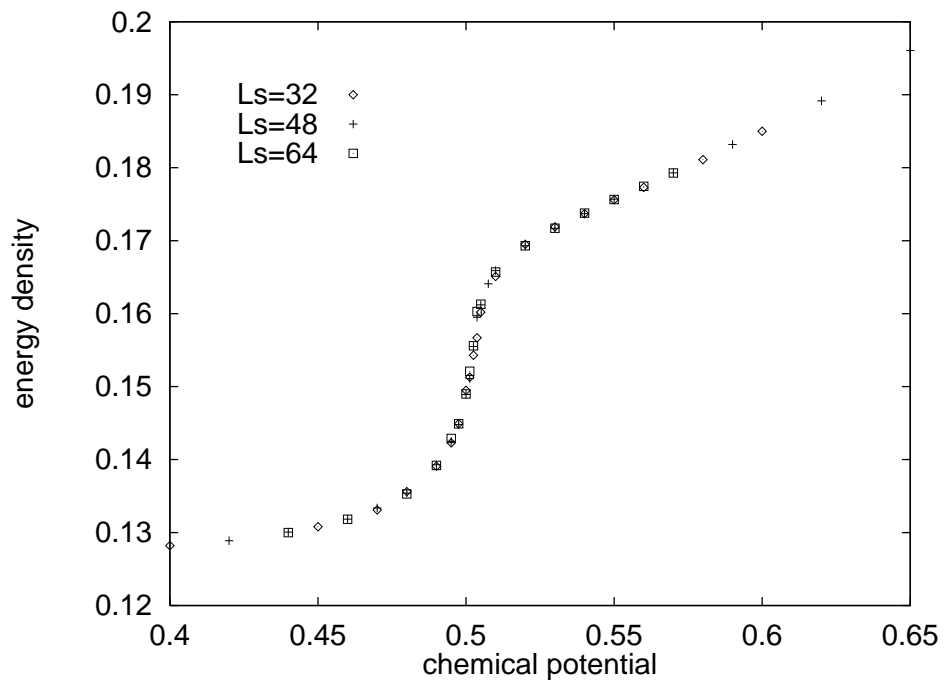


FIG. 17. Energy density E vs. μ for $L_t = 16$, $\beta = 0.55$ and $L_s = 32, 48, 64$.

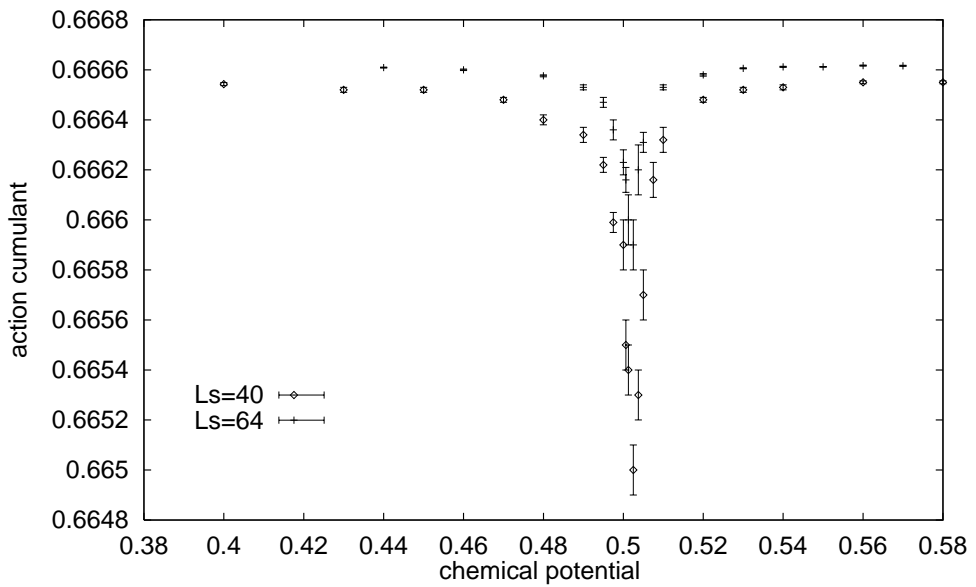
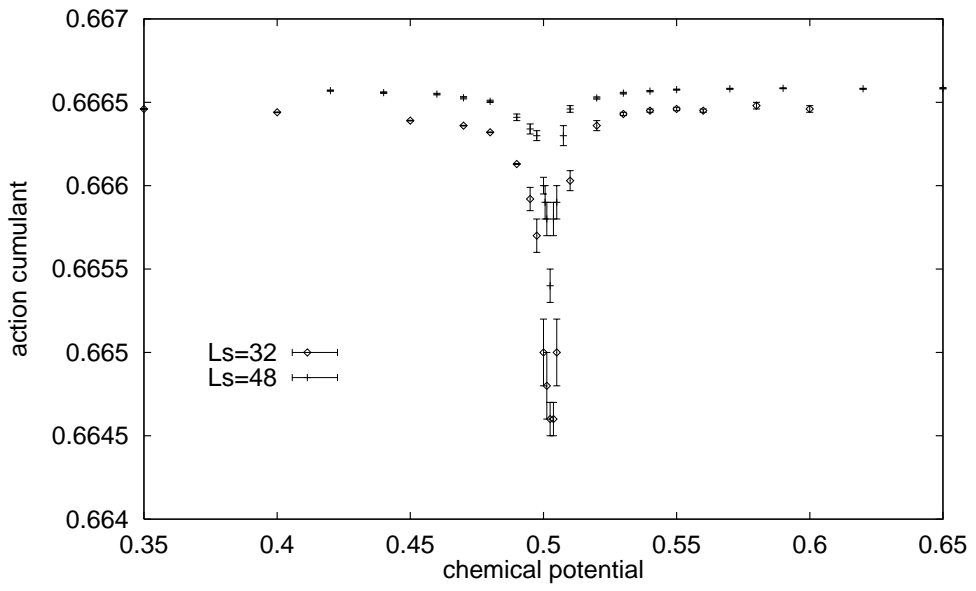


FIG. 18. The action cumulant B_S vs. μ for $L_t = 16, \beta = 0.55$ and $L_s = 32, 40, 48, 64$.

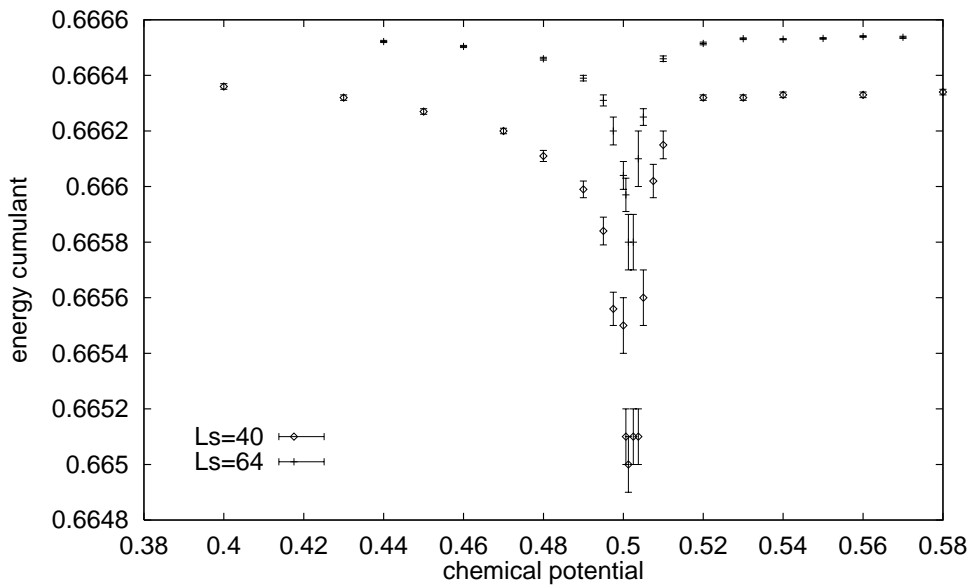
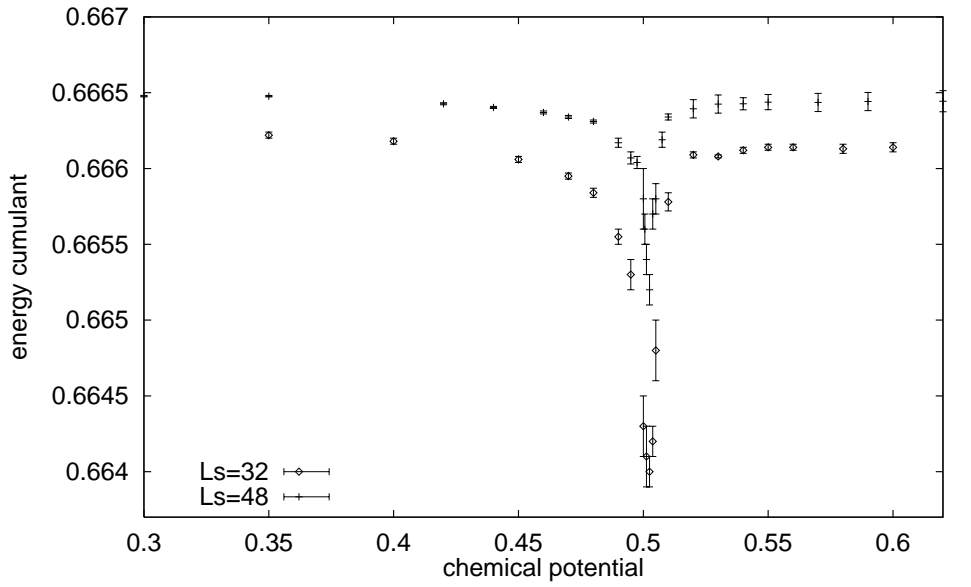


FIG. 19. The energy cumulant B_E vs. μ for $L_t = 16$, $\beta = 0.55$ and $L_s = 32, 40, 48, 64$.

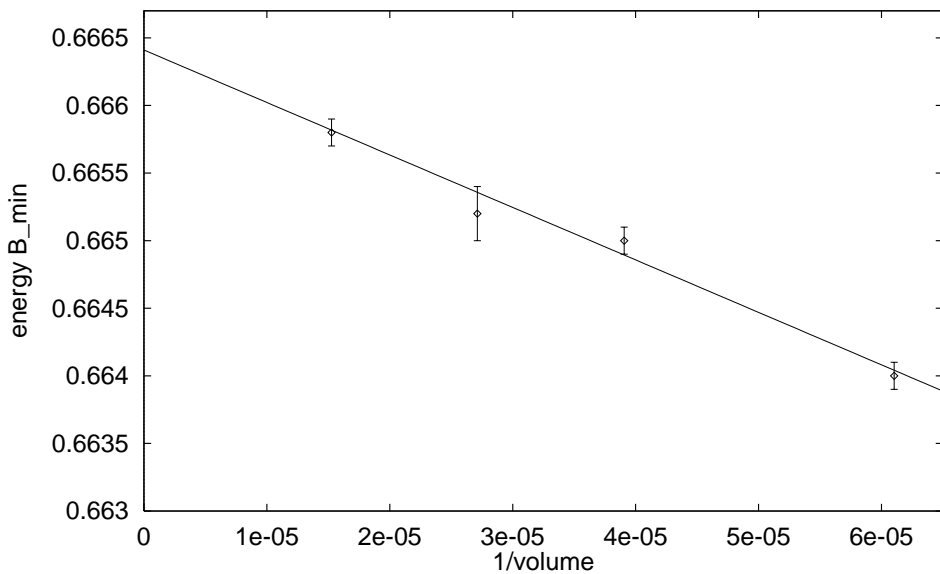
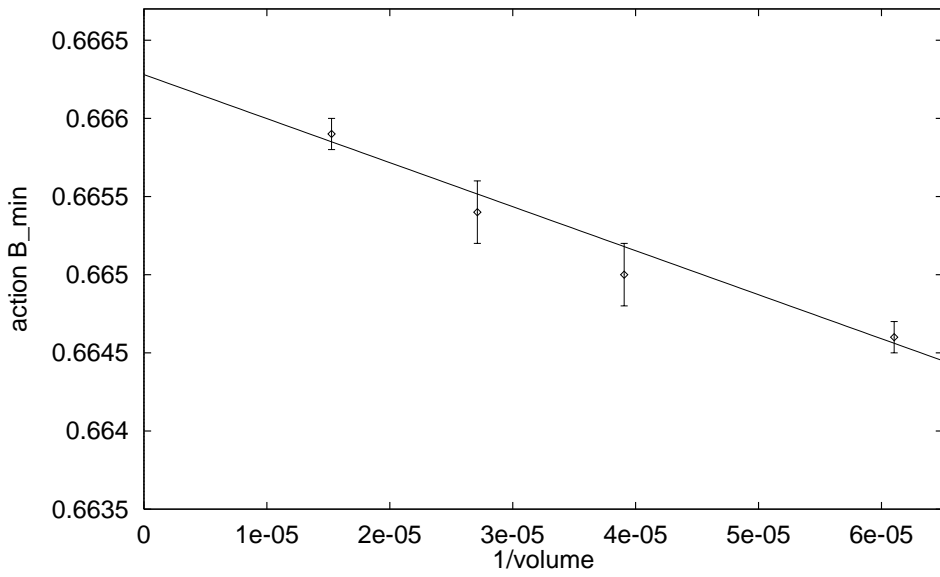


FIG. 20. The minimum values of the action and energy cumulants vs. inverse volume for $L_t = 16, \beta = 0.55$. The solid lines represent the best linear fits to the data.